Biochimica et Biophysica Acta 1838 (2014) 822–830

Contents lists available at ScienceDirect

Biochimica et Biophysica Acta

journal homepage: www.elsevier.com/locate/bbamem

Ca^{2+} induces $PI(4,5)P_2$ clusters on lipid bilayers at physiological $PI(4,5)P_2$ and Ca^{2+} concentrations

Maria J. Sarmento [a], Ana Coutinho [a,b], Aleksander Fedorov [a], Manuel Prieto [a], Fabio Fernandes [a,*]

[a] Centro de Química-Física Molecular and Institute of Nanoscience and Nanotechnology, Instituto Superior Técnico, University of Lisbon, Lisbon, Portugal
[b] Departamento de Química e Bioquímica, FCUL, University of Lisbon, Lisbon, Portugal

ARTICLE INFO

Article history:
Received 23 July 2013
Received in revised form 22 November 2013
Accepted 26 November 2013
Available online 6 December 2013

Keywords:
Fluorescence spectroscopy
FRET
FCS
Calcium
$PI(4,5)P_2$

ABSTRACT

Calcium has been shown to induce clustering of $PI(4,5)P_2$ at high and non-physiological concentrations of both the divalent ion and the phosphatidylinositol, or on supported lipid monolayers. In lipid bilayers at physiological conditions, clusters are not detected through microscopic techniques. Here, we aimed to determine through spectroscopic methodologies if calcium plays a role in $PI(4,5)P_2$ lateral distribution on lipid bilayers under physiological conditions. Using several different approaches which included information on fluorescence quantum yield, polarization, spectra and diffusion properties of a fluorescent derivative of $PI(4,5)P_2$ (TopFluor(TF)-$PI(4,5)P_2$), we show that Ca^{2+} promotes $PI(4,5)P_2$ clustering in lipid bilayers at physiological concentrations of both Ca^{2+} and $PI(4,5)P_2$. Fluorescence depolarization data of TF-$PI(4,5)P_2$ in the presence of calcium suggests that under physiological concentrations of $PI(4,5)P_2$ and calcium, the average cluster size comprises ~15 $PI(4,5)P_2$ molecules. The presence of Ca^{2+}-induced $PI(4,5)P_2$ clusters is supported by FCS data. Additionally, calcium mediated $PI(4,5)P_2$ clustering was more pronounced in liquid ordered (l_o) membranes, and the $PI(4,5)P_2$-Ca^{2+} clusters presented an increased affinity for l_o domains. In this way, $PI(4,5)P_2$ could function as a lipid calcium sensor and the increased efficiency of calcium-mediated $PI(4,5)P_2$ clustering on l_o domains might provide targeted nucleation sites for $PI(4,5)P_2$ clusters upon calcium stimulus.

1. Introduction

Cells spend a significant amount of energy in order to maintain the intracellular calcium levels at a very low range (~100 nM, while the extracellular concentration is typically 1–3 mM), pumping Ca^{2+} ions to internal storage organelles as the endoplasmic reticulum or to the extracellular space. A low cytosolic Ca^{2+} concentration is particularly important for highly specialized cells like neurons, since it allows a fast and effective response to the influx of Ca^{2+} after stimulation [1,2].

In pre-synaptic terminals, the process of synaptic vesicle fusion begins with an action potential, during which the membrane quickly depolarizes. Membrane depolarization leads to calcium influx by opening of voltage-gated Ca^{2+} channels. Inside the cells, calcium diffusion is severely limited due to the presence of mobile and immobile calcium buffers [3] and, as a result, a highly transient and localized microdomain of increased calcium concentration is formed around open calcium channels. Peak concentration in the mouth of an open channel is expected to reach hundreds of μM, several orders of magnitude higher than those of the average intracellular calcium concentrations. The presence of molecular calcium targets in close vicinity to the calcium channels allows for fast and selective activation, and therefore, a downstream synchronized vesicle fusion with the plasma membrane takes place with the consequent release of neurotransmitters [1,4].

Phosphatidylinositol 4,5-bisphosphate ($PI(4,5)P_2$), has been shown to be a key player in the regulation of exocytosis [5–8]. A recent study showed that $PI(4,5)P_2$ increased synaptotagmin sensitivity for Ca^{2+} more than 40-fold [8]. $PI(4,5)P_2$ is a minor component of the inner leaflet of the plasma membrane of eukaryotic cells, comprising around 1 mol% of the total membrane phospholipids [9,10], and is essential for several cellular mechanisms besides exocytosis, including organization and remodeling of the actin cytoskeleton [11–14], membrane trafficking (reviewed in [15]) and endocytosis [16–18]. In exocytosis, the size of the readily releasable vesicle pools was found to scale with the amount of $PI(4,5)P_2$ in the plasma membrane [19].

A possible explanation for such dramatic influence of $PI(4,5)P_2$ on membrane fusion sensitivity to calcium lies on the recent observation that Ca^{2+} had an active role in the modulation of $PI(4,5)P_2$ lateral organization. Calcium ions have already been shown to promote the formation of large $PI(4,5)P_2$ clusters, visible under the microscope in membrane model systems at very high $PI(4,5)P_2$ levels (5–50% molar fraction), or at non-physiological calcium concentrations (~1 mM) [20–23] as most $PI(4,5)P_2$ resides on the inner bilayer leaflet, not exposed to high extracellular calcium concentration. The mechanism behind the creation of these structures is the formation of crossbridges between divalent cations and the polyanionic headgroup of this phosphoinositide [20]. In fact, at low

* Corresponding author. Tel.: +351 218 419 219; fax: +351 218 464 455.
E-mail address: fernandesf@ist.utl.pt (F. Fernandes).

0005-2736/$ – see front matter © 2013 Elsevier B.V. All rights reserved.
http://dx.doi.org/10.1016/j.bbamem.2013.11.020

pH values corresponding to a PI(4,5)P_2 monovalent headgroup, the formation of visible PI(4,5)P_2 clusters is abrogated [21].

In a recent work [23], Wang and coworkers observed clustering of PI(4,5)P_2 at near physiological conditions in supported lipid monolayer systems. At variance, in the present work, free-standing lipid bilayers under no perturbation are studied using membrane model systems containing physiological concentrations of a PI(4,5)P_2 fluorescent analog. Several fluorescence spectroscopy methodologies, as well as fluorescence correlation spectroscopy (FCS), are employed to study the clustering of PI(4,5)P_2 molecules in the presence of Ca^{2+} at physiological concentrations (μM range).

The spectroscopic approach used in this study allowed the detection and characterization of both diffusion and length scales associated with calcium-dependent PI(4,5)P_2 clusters. Additionally, the influence of membrane lipid phase on the efficiency of calcium-mediated PI(4,5)P_2 clustering was also studied, since PI(4,5)P_2 spatial distribution is often intrinsically associated with cholesterol-dependent membrane rafts [24–26].

2. Material and methods

2.1. Materials

1-Palmitoyl-2-oleoyl-*sn*-glycero-3-phosphocholine (POPC), N-palmitoyl-D-*erythro*-sphingosylphosphorylcholine (PSM), 1,2-dioleoyl-*sn*-glycero-3-phosphoethanolamine-N-(cap biotinyl) (DOPE-Cap-biotin), 1-oleoyl-2-{6-[4-(dipyrrometheneboron difluoride) butanoyl] amino} hexanoyl-*sn*-glycero-3-phosphoinositol-4,5-bisphosphate (TF-PI(4,5)P_2), 1,2-dioleoyl-*sn*-glycero-3-phospho-(1′-myo-inositol-4′,5′-bisphosphate) (PI(4,5)P_2) and 1-palmitoyl-2-(dipyrrometheneboron difluoride) undecanoyl-*sn*-glycero-3-phospho-L-serine (TF-POPS) were obtained from Avanti Polar Lipids (Alabaster, AL). Avidin from egg white and cholesterol (Chol) were from Sigma Chemical Co. (St. Louis, MO). Rhodamine 110 and Fluo-5N were obtained from Molecular Probes, Invitrogen (Eugene, OR). All organic solvents were UVASOL grade from Merck (Darmstadt, Germany).

2.2. Liposome preparation

Large unilamellar vesicles (LUVs) were prepared by extrusion of multilamellar vesicles [27]. Briefly, lipid mixtures composed of the adequate amounts of lipids and TF-PI(4,5)P_2 were prepared in chloroform to a final lipid concentration of 0.5 mM. The solvent was slowly vaporized under a nitrogen flux and the resulting lipid film was left in vacuum overnight to ensure the complete removal of the organic solvent. Afterwards, the lipid was re-suspended in 700 μL of a 10 mM HEPES buffer (pH 7.4), containing 150 mM NaCl and the desired $CaCl_2$ concentration. Freeze-thaw cycles (liquid nitrogen/water bath at 60 °C) were then performed to re-equilibrate and homogenize the samples. LUVs were finally obtained by extrusion of the solutions at 50 °C with an Avanti Mini-Extruder (Alabaster, AL) using 100 nm pore size polycarbonate membranes. Measurements were carried out at 0.25 mM total lipid concentration. Controls were performed replacing TF-PI(4,5)P_2 with TF-POPS.

Giant unilamellar vesicles (GUVs) were obtained by electroformation in Pt wires as previously described [28,29]. Briefly, lipid solutions were prepared in chloroform (from lipid stock solutions) to a final lipid concentration of 1 mM. All mixtures were composed of POPC or POPC: PI(4,5)P_2 99:1 (mol:mol). In order to immobilize GUVs in an avidin coated surface for imaging, DOPE-Cap-biotin was included at a biotinylated lipid/total lipid ratio of $1/10^6$ [30]. For the confocal microscopy measurements, TF-PI(4,5)P_2 was added at a probe/lipid ratio of 1/500 (0.2 mol%). To perform FCS, TF-PI(4,5)P_2 was present at a 1/50,000 probe/lipid ratio (0.002 mol%). After removal of the solvent, electroformation was performed at 58 °C during 75 min, in 1 mL of a 200 mM sucrose solution preheated at the same temperature. Then, 150 μL of the GUV solution were transferred to a μ-Slide from Ibidi (Munich, Germany) coated with avidin and a 200 mM glucose solution was also added to the wells in order to increase GUV deposition and immobilization rate.

All calcium concentrations were controlled using the calcium indicator Fluo-5N, following the instructions of the manufacturer; the buffer with no free calcium ions was prepared with 5 mM EDTA.

Lipid stock solutions were all prepared in chloroform, with the exception of PI(4,5)P_2 and TF-PI(4,5)P_2 that were prepared in chloroform/methanol (2:1). POPC, PSM and DOPE-Cap-biotin concentrations in the stock solutions were determined using an inorganic phosphate colorimetric quantification method [31]. Cholesterol concentration was determined by gravimetry (Mettler Toledo UMT2). Determination of probe concentrations was performed spectrophotometrically using ε(TF-PI(4,5)P_2, 495 nm, methanol) = 80×10^3 M^{-1} cm^{-1} (Bodipy [32]) and ε(TF-POPS, 495 nm, methanol) = 80×10^3 M^{-1} cm^{-1} (Bodipy [32]).

2.3. Steady-state fluorescence spectroscopy

Fluorescence measurements were carried out with a SLM-Aminco 8100 Series 2 spectrofluorimeter (Rochester, NY) with double excitation and emission monochromators (MC-400), in right-angle geometry. The light source was a 450-W Xe arc lamp and the reference a Rhodamine B quantum counter solution. Quartz cuvettes (0.5 × 0.5 cm) from Hellma Analytics were used. Temperature was controlled to 25 °C.

Fluorescence intensities were corrected for inner filter effects according to [33]. Steady-state fluorescence anisotropy, $\langle r \rangle$ is defined as [34]:

$$\langle r \rangle = \frac{I_{VV} - G I_{VH}}{I_{VV} + 2G I_{VH}} \quad (1)$$

where I_{VV} and I_{VH} are the steady-state vertical and horizontal components of fluorescence emission, respectively, with excitation accomplished with vertically polarized light. The components with excitation horizontal to the emission axis, I_{HV} and I_{HH}, are used to calculate the *G* factor:

$$G \frac{I_{HV}}{I_{HH}}. \quad (2)$$

For the polarization of excitation and emission light, Glan–Thompson polarizers were used. Blank subtraction was taken into account in all anisotropy components, as well as in the other fluorescence intensity measurements.

2.4. Time-resolved fluorescence spectroscopy

Fluorescence decay measurements were carried out making use of the Time-Correlated Single-Photon Timing (TCSPT) technique, as described elsewhere [35]. TF-PI(4,5)P_2 was excited at 460 nm, and fluorescence emission was acquired at 505 nm. The emission wavelength was selected by a Jobin Yvon HR320 monochromator (Horiba Jobin Ivon Inc.). 0.5 × 0.5-cm quartz cuvettes from Hellma Analytics were used. Blank decays were acquired and photon counts were negligible.

The fluorescence intensity decays were described by a sum of exponentials:

$$i(t) = \sum_i \alpha_i exp(-t/\tau_i) \quad (3)$$

where α_i is the normalized amplitude and τ_i is the *i*th component lifetime. The amplitude-weighted average lifetime is defined by:

$$\overline{\tau} = \sum_i \alpha_i \tau_i. \quad 4$$

Data analysis was performed with the TRFA software (Scientific Software Technologies Center, Minsk, Belarus) based on the Levenberg–

Marquardt algorithm. The goodness of the fit was judged from the experimental χ^2 weighted residuals and autocorrelation plot. In every analysis, χ^2 was less than 1.3 and both residuals and autocorrelation were randomly distributed around zero.

2.5. Confocal fluorescence microscopy

All measurements were performed on a Leica TCS SP5 (Leica Microsystems CMS GmbH, Mannheim, Germany) inverted confocal microscope (DMI6000). A 63× apochromatic water immersion objective with a NA of 1.2 (Zeiss, Jena Germany) was used for all experiments, and an Argon laser was used for excitation.

$CaCl_2$ was always added to the desired concentration after GUV immobilization.

Images were acquired at 400 Hz, exciting TF-PI(4,5)P_2 at 488 nm and collecting emission between 495 and 530 nm. For each GUV top hemisphere, *xy* slices separated by 0.4 μm were acquired and then converted in a *xy* projection, making use of the maximum intensity projection method [36]. Projections were made using ImageJ (Wayne Rasband, NIH, USA).

2.6. Fluorescence correlation spectroscopy

FCS measurements were carried out using the same optical path described for the confocal imaging, except that fluorescence emission was detected using avalanche photodiodes (APDs) after passing through a 500–550 band-pass filter. Excitation of the TF fluorophore was performed with the 488 nm line of the argon laser. The dimensions of the focal volume were determined by calibration with rhodamine 110 (5 nM and 10 nM) in milliQ water using the same optical setup as the samples. A rhodamine 110 diffusion coefficient (D) of 440 $\mu m^2 s^{-1}$ was considered [37]. The beam waist of the laser focus, ω_0, was calculated and then fixed in all the subsequent analysis of samples measured in the same μ-Slide.

For each calcium concentration, $CaCl_2$ was added to the μ-Slide chambers after GUV immobilization and the lateral diffusion of TF-PI(4,5)P_2 in at least six different immobilized GUVs was measured by point FCS as previously described [38,39]. Five autocorrelation curves, $G(\tau)$, were sequentially obtained in each vesicle, with an acquisition time of 20 s and a 100 kHz sampling frequency. The fit to each autocorrelation curve was accomplished with a 2D Gaussian model [40]:

$$G(\tau) = \frac{1}{C\pi\omega_0^2}\left(1 + \frac{4D\tau}{\omega_0^2}\right)^{-1} \quad (5)$$

where C is the surface concentration, D is the fluorescent phospholipid diffusion coefficient and τ is the lag time.

3. Results

3.1. Lateral distribution of TF-PI(4,5)P_2 in fluid membranes

In order to study the lateral distribution of PI(4,5)P_2 in lipid membranes, TF-PI(4,5)P_2 was chosen. In this molecule, PI(4,5)P_2 is labeled with a dipyrromethene boron difluoride moiety on the short fatty acid chain in the *sn*2-position. Labeling in the acyl-chain was required in order to prevent modification of the inositol ring. Additionally, this fluorophore exhibits significant efficiency for self-quenching at high concentrations, providing an excellent tool to detect changes in the distribution of the labeled lipid in the lipid membrane [41].

LUVs composed of POPC were prepared with 0.1, 0.25, 0.5, 1.0 and 2.0 mol% TF-PI(4,5)P_2 to characterize the fluorescence emission properties of the fluorescently labeled phosphoinositol (Fig. 1A). We observed that fluorescence intensity scaled linearly with TF-PI(4,5)P_2 concentration up to 1 mol% of analog molar fraction (Fig. 1B). Above this concentration a minor negative deviation is observed. An identical behavior had been previously observed for a similar PI(4,5)P_2 fluorescent analog [20]. This non-linear relationship indicates that fluorescence self-quenching occurs when high concentrations of the probe are present. Since this decrease in fluorescence quantum yield above 1 mol% TF-PI(4,5)P_2 cannot be rationalized on the basis of collisional

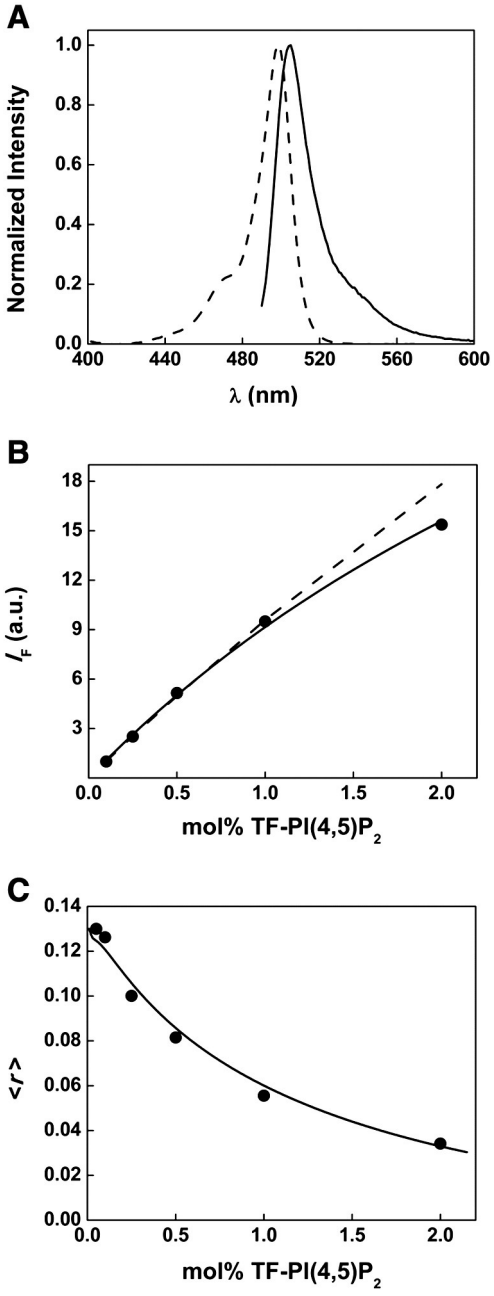

Fig. 1. TF-PI(4,5)P_2 does not aggregate (<1%) in fluid membranes. Fluorescence properties of TF-PI(4,5)P_2 in the absence of calcium and within LUVs containing different concentrations of TF-PI(4,5)P_2. (A) Normalized absorption (—) and emission (—) spectra of TF-PI(4,5)P_2 (1 mol%) incorporated in POPC vesicles. Maximum absorption and emission wavelengths are 499 nm and 505 nm, respectively. (B) Steady-state fluorescence intensity measurements of TF-PI(4,5)P_2 at different concentrations (●). Expected steady-state fluorescence intensities in the presence of collisional quenching between freely diffusing TF-PI(4,5)P_2 molecules and absence of nonfluorescent dimers (—). A model for dark dimer formation is also fitted to the data (—) (Appendix). (C) Steady-state fluorescence anisotropy of TF-PI(4,5)P_2 upon increase of its surface concentration (●). The Snyder and Freire fluorescence depolarization model [42] derived for a random surface distribution of fluorophores undergoing energy migration in a lipid membrane was fitted to the data (—) (see the Appendix for details on this model). (B) and (C) represent averages of three experiments; standard deviation bars are smaller than the respective symbols.

quenching between freely diffusing TF-PI(4,5)P_2 molecules (Fig. 1B, see the Appendix for details), a small concentration-dependent tendency for the formation of dark dimers or other small complexes (static quenching) must be present. Formation of ground state nonfluorescent dimers has been reported for other lipid derivatives of dipyrromethene boron difluoride at very high densities in lipid membranes [42,43]. The observation of static quenching at molar fractions of TF-PI(4,5)P_2 higher than 1 mol% is likely to result from the formation of such dimers, since fluorescence from fluorescent dimers (typically observed at 630 nm [43]) is not observed. Additionally, significant spontaneous aggregation of PI(4,5)P_2 on fluid POPC bilayers in the absence of calcium, has been previously ruled-out [44,45]. Assuming that nonfluorescent dimers are the only oligomers formed, a dimerization constant (K_A) can be recovered from the fluorescence data (see Appendix), and $K_A = 5.93\ M^{-1}$ was obtained (Fig. 1B). Effective concentrations of TF-PI(4,5)P_2 in the membrane were used as described elsewhere [46]. The very low K_A value recovered confirms that TF-PI(4,5)P_2 has very low affinity for aggregation in the absence of calcium.

The TF fluorophore of TF-PI(4,5)P_2 monomers is capable of energy transfer (homotransfer or energy migration) to other TF-PI(4,5)P_2 monomers in its vicinity. As a result, fluorescence depolarization takes place, and the fluorescence anisotropy ($\langle r \rangle$) of the molecule becomes highly sensitive to the surface density of TF-PI(4,5)P_2. In the case of TF, energy transfer is highly efficient, given the small Stokes-shift of the molecule (Fig. 1A). The Förster radius (R_0) for energy migration of TF-PI(4,5)P_2 is a measure of the efficiency of energy transfer, and was determined by us as described elsewhere [47] to be $R_0 = 56$ Å. The expected fluorescence depolarization as a result of energy migration (for a particular R_0) for a homogeneous distribution of molecules within lipid membranes can be determined as described in the Appendix [48]. The comparison of these expected values for fluorescence depolarization in the absence of heterogeneities with the experimentally obtained fluorescence emission anisotropies of TF-PI(4,5)P_2 in the absence of calcium (Fig. 1C) confirms that, in fluid POPC bilayers, TF-PI(4,5)P_2 is mostly monodispersed and no significant aggregation or segregation within the bilayer takes place below 1% molar fraction of PI(4,5)P_2. Nevertheless, given the aggregation observed at high molar fractions of PI(4,5)P_2, it is likely that a very small fraction of the phospholipid is found aggregated below 1 mol%, even in the absence of calcium.

3.2. Calcium regulation of PI(4,5)P_2 organization in fluid lipid bilayers at physiological concentrations of PI(4,5)P_2 and Ca^{2+}

POPC and POPC:PI(4,5)P_2 99:1 (mol:mol) GUVs were prepared with 0.2 mol% of the fluorescently labeled phosphoinositide. After vesicle immobilization, the desired calcium concentration was achieved through addition of a concentrated calcium solution, and GUVs were imaged by confocal fluorescence microscopy (Fig. 2). Clearly, at physiological concentrations of PI(4,5)P_2, no macroscopic TF-PI(4,5)P_2 clustering is visible either in the absence or presence of calcium (up to 100 μM). At 1 mol% PI(4,5)P_2 (Fig. 2D-F), even non-physiological calcium concentrations were ineffective in producing macroscopic clusters (Fig. A1 in the Appendix). The absence of detectable PI(4,5)P_2 clusters in these measurements implies that either PI(4,5)P_2 distribution is insensitive to the presence of calcium at physiological concentrations or that any heterogeneities formed are below the resolution of the confocal microscope.

In order to clarify this, a spectroscopic characterization of TF-PI(4,5)P_2 in POPC liposomes was conducted in the presence of 0–100 μM Ca^{2+}. Total PI(4,5)P_2 concentration was always kept within physiological concentrations (≤1 mol%) and controls with the anionic fluorescent analog TF-POPS were always performed. Fluorescence emission spectra were recorded for the different calcium concentrations (Fig. 3A). Calcium induced a dramatic decrease in TF-PI(4,5)P_2 quantum yield for different concentrations of the fluorescent analog. This decrease can only be rationalized on the basis of TF-PI(4,5)P_2 clustering. As the fluorescence data clearly show, clustering sensitivity for calcium was strongly associated with the concentration of the fluorescent phosphoinositol (Fig. 3B). When POPC LUVs were loaded with 0.1 mol% TF-PI(4,5)P_2 and 0.9 mol%

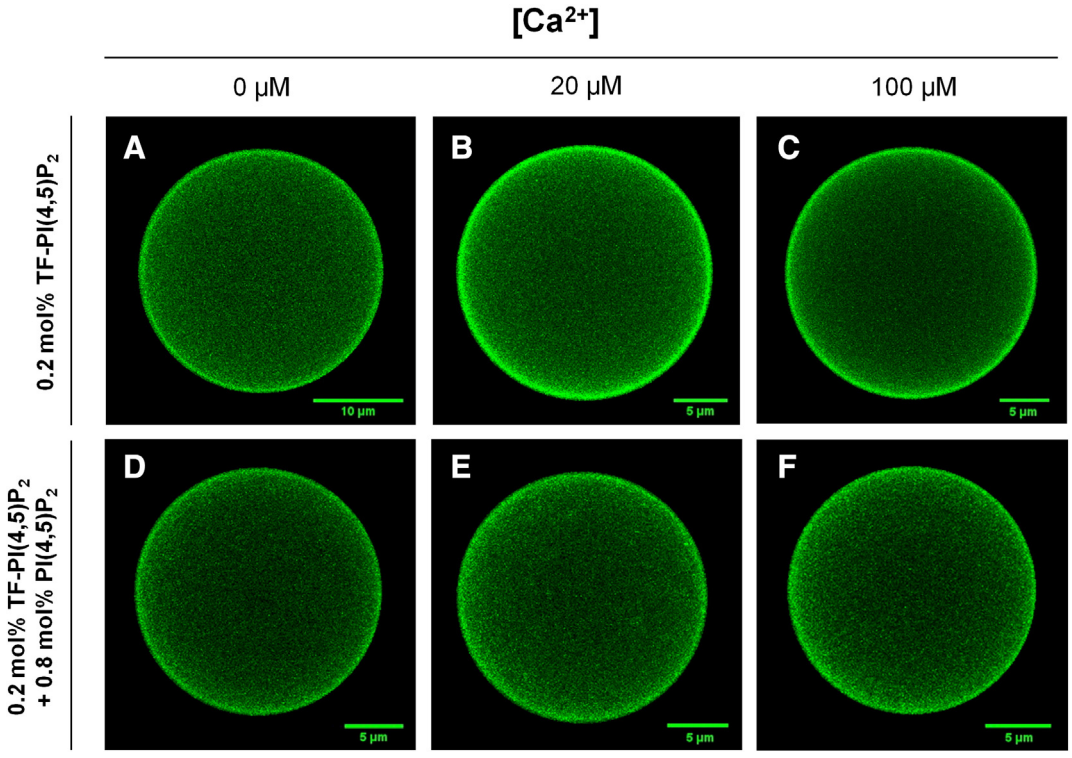

Fig. 2. Calcium does not induce the formation of macroscopic PI(4,5)P_2 aggregates at physiologic concentrations. GUVs were formed containing POPC:TF-PI(4,5)P_2 99.8:0.2 (mol:mol) (A–C) and POPC:PI(4,5)P_2:TF-PI(4,5)P_2 99:0.8:0.2 (mol:mol:mol) (D–F). Different physiologically relevant calcium concentrations were externally added after vesicle immobilization. Confocal imaging was accomplished through excitation at 488 nm and emission collection in the 495–530 nm range. Examples of the obtained maximum intensity projections of the top hemispheres are depicted.

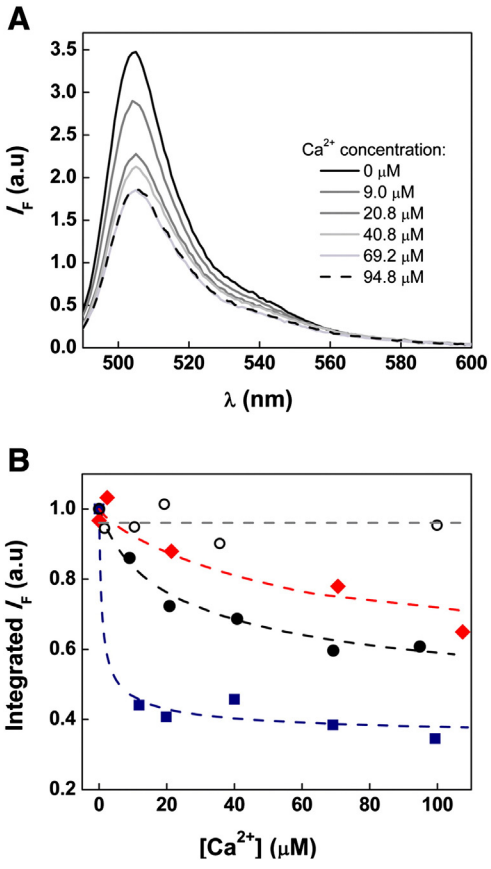

Fig. 3. Calcium induces aggregation of TF-PI(4,5)P_2 at physiological concentrations. Fluorescence emission measurements of TF-PI(4,5)P_2 were carried out within POPC LUVs (0.25 mM) in buffers containing distinct calcium concentrations. (A) Fluorescence emission spectra of LUVs containing 0.1 mol% TF-PI(4,5)P_2 in the presence of increasing calcium concentrations. (B) Integrated fluorescence emission of LUVs containing 0.1 mol% (●) and 1 mol% (■) TF-PI(4,5)P_2, and also 0.1 mol% TF-PI(4,5)P_2 loaded with non-labeled PI(4,5)P_2 to a total of 1 mol% phosphoinositide (◆). TF-POPS (1 mol%) was used as a control (○). Dashed lines are guides to the eye.

unlabeled PI(4,5)P_2 (1 mol% total PI(4,5)P_2), the calcium-induced fluorescence quenching decreased significantly, confirming that the decrease in TF-PI(4,5)P_2 quantum yield is a result of PI(4,5)P_2-PI(4,5)P_2 interactions. In this case, the probability of TF contacts to occur within aggregates is reduced through dilution of the fluorescent phosphoinositol with unlabeled molecules. Additionally, TF-POPS at 1% molar fraction is almost insensitive to calcium concentrations below 100 μM. In this way, calcium is far less effective in generating PS clusters in the physiological range of concentrations of the divalent cation.

Ca^{2+} also promoted a depolarization of fluorescence emission of TF-PI(4,5)P_2 as seen on Fig. 4. This is evident both from steady-state anisotropies (Fig. 4A) as from anisotropy decays (Fig. 4B). This depolarization can only be rationalized on the basis of PI(4,5)P_2 clustering in the membrane and the consequent increase in local TF-PI(4,5)P_2 concentrations. In order to improve the sensitivity of the assay for aggregation, a small concentration of TF-PI(4,5)P_2 was employed (0.1 mol%). As seen from Fig. 1C, sensitivity for TF-PI(4,5)P_2 concentration was maximum at very low concentrations of the labeled phospholipid. In fact, significant calcium-induced fluorescence depolarization is only observed for low concentrations (0.1 mol%) of the fluorescent inositol (Fig. 4A,B), since at higher concentrations (1 mol%), the fluorescence anisotropy becomes largely insensitive to the membrane concentration (Fig. 4A,D) and, as seen before, monomer quantum yield is significantly higher than the quantum yield of aggregated molecules. Additionally, since calcium also induced a significant decrease in the fluorescence lifetime of TF-PI(4,5)P_2 at 1 mol% (Fig. A2 in the Appendix), it is possible that the decrease in fluorescence anisotropy due to energy migration is balanced at high TF-PI(4,5)P_2 concentrations by the increase in anisotropy associated with a lower lifetime for rotation.

Importantly, in the presence of calcium, fluorescence depolarization increased significantly when unlabeled PI(4,5)P_2 was added to the liposomes to increase total inositol concentration (Fig. 4A,D). In the absence of the divalent cation, fluorescence anisotropy was insensitive to the presence of unlabeled PI(4,5)P_2 (Fig. 4D, inset). TF-POPS fluorescence was also insensitive to this effect (results not shown). Interestingly, calcium induced fluorescence depolarization of TF-PI(4,5)P_2 is insensitive to the presence of a high concentration of polyamines such as spermidine (Fig. A3 in the Appendix), suggesting a higher affinity of PI(4,5)P_2 for calcium than for polyamines.

Since PI(4,5)P_2 diameter (L) << $R_{0(\text{TF-PI(4,5)P2})}$, energy migration between fluorophores within the same aggregate induces a decrease in fluorescence anisotropy which is constant for a given number s of fluorophores within the aggregate [49]. With this information, it is possible to estimate through a binomial distribution the effect of energy migration on the fluorescence anisotropy of the sample with a mixed TF-PI(4,5)P_2/PI(4,5)P_2 population for different cluster sizes (see the Appendix for details), taking into account the fraction of aggregated inositol obtained from the fluorescence self-quenching data. Simulations for fluorescence depolarization of TF-PI(4,5)P_2 when diluted with nonfluorescent PI(4,5)P_2 in case only small aggregates are formed ($s \leq 4$), show that virtually unchanged fluorescence anisotropies are expected, as the probability of finding multiple labeled molecules is reduced (Fig. 4C). As such, the observed decrease in fluorescence depolarization in the presence of calcium and unlabeled PI(4,5)P_2 can only be the result of significant sized clusters. In fact, fluorescence depolarization data for the mixed TF-PI(4,5)P_2/PI(4,5)P_2 sample in the presence of calcium was accurately modeled when assuming a cluster size $s = 15$. This is an average value, since the dimensions of PI(4,5)P_2 clusters are probably dependent on Ca^{2+} concentrations, but it illustrates that at physiological concentrations of both PI(4,5)P_2 and calcium, an increase in the concentration of the divalent ion sustains the formation of platforms of PI(4,5)P_2 in the membrane.

In the presence of Ca^{2+}, a change in the fluorescence emission spectrum of TF is also observed (Fig. A4.A in the Appendix). This alteration in TF emission is more clearly identified through the ratio of fluorescence emission intensity at 505 (maximum emission) and 570 nm (Fig. A4.B in the Appendix). These changes in TF-PI(4,5)P_2 fluorescence emission spectrum shape cannot be ascribed to the formation of fluorescent excimers of TF within PI(4,5)P_2 aggregates, since these have been reported to emit at much longer wavelengths (~630 nm) [42,43], and no increase in emission at this wavelength is observed (results not shown). Additionally, no changes in absorption spectra are detected in the presence of calcium (results not shown). As such, this small spectral change is in fact also reporting energy transfer from fluorescent TF-PI(4,5)P_2 to clustered TF-PI(4,5)P_2 complexes, which is more effective for a blue-shifted fraction of TF-PI(4,5)P_2 (the fluorescence spectrum of TF-PI(4,5)P_2 constitutes a heterogeneous distribution), as described elsewhere [42]. Once more, this effect of calcium was selective for PI(4,5)P_2, as TF-POPS fluorescence emission spectrum was totally insensitive even at 1 mol% TF-POPS (Fig. A4.B in the Appendix).

In case that large clusters of PI(4,5)P_2 are formed, the diffusion properties of these aggregates are expected to be changed to some extent. To follow these changes, we performed point FCS in POPC GUVs containing 0.002 mol% TF-PI(4,5)P_2 and non-labeled PI(4,5)P_2 to complete 1% of total PI(4,5)P_2 molar fraction (Fig. 5). Very small concentrations of fluorophore are used to ensure that fluorescence bursts arising from near single-molecule detection have maximum contrast during acquisition.

The diffusion coefficient of TF-PI(4,5)P_2 decreased to some extent with calcium, going from 8.01 ± 0.13 $\mu m^2 s^{-1}$ in the absence of calcium to 6.58 ± 0.20 $\mu m^2 s^{-1}$ at 100 μM Ca^{2+} (D ± SEM). The diffusion coefficient obtained for TF-PI(4,5)P_2 in the absence of calcium is consistent with the values of 7.7–10 μm^2 s^{-1} reported for another fluorescent

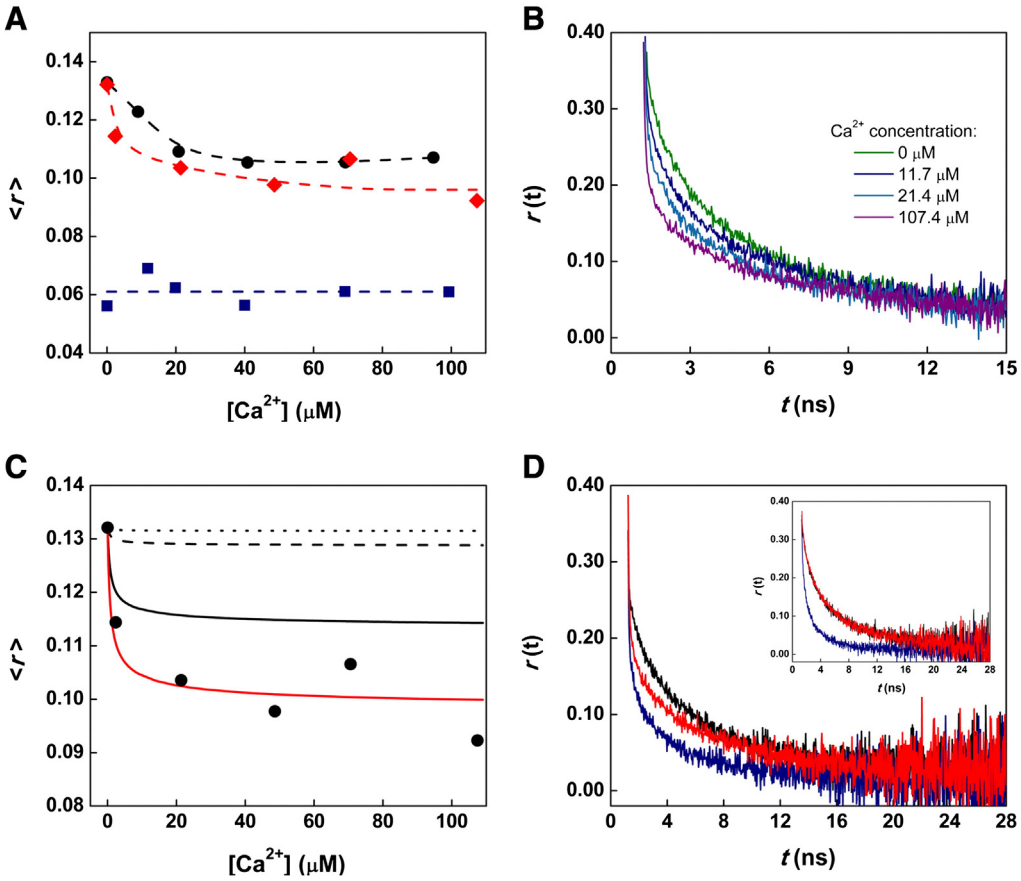

Fig. 4. Calcium induces the formation of large $PI(4,5)P_2$ clusters. Fluorescence anisotropy measurements were performed using POPC vesicles with different mol% of TF-$PI(4,5)P_2$, with (0.9 mol%) and without non-labeled $PI(4,5)P_2$. (A) Effect of increasing calcium concentrations on the steady-state anisotropy of vesicles containing 0.1 mol% (●) and 1 mol% (■) TF-$PI(4,5)P_2$, and also 0.1 mol% TF-$PI(4,5)P_2$ loaded with unlabeled $PI(4,5)P_2$ to a total of 1 mol% phosphatidylinositol (◆). Dashed lines are guides to the eye. (B) Time-resolved fluorescence anisotropy of vesicles containing TF-$PI(4,5)P_2$ (0.1 mol%) and $PI(4,5)P_2$ (1 mol% total phosphoinositol), in the absence (green) and presence of 11.7 μM (dark blue), 21.4 μM (blue) and 107.4 μM (purple) of Ca^{2+}. (C) An oligomerization model was used to analyze the fluorescence anisotropy data from POPC liposomes containing 0.1 mol% of TF-$PI(4,5)P_2$ and 0.9 mol% $PI(4,5)P_2$ (●). Through a binomial distribution, the effect of energy migration between TF-$PI(4,5)P_2$ fluorescent molecules on the fluorescence anisotropy were calculated considering oligomer sizes of $s = 2$ (dotted line), $s = 4$ (dashed line), $s = 10$ (black full line) and $s = 15$ (red full line) (see the Appendix for details). (D) Time-resolved fluorescence anisotropy of vesicles with 0.1 mol% TF-$PI(4,5)P_2$ (black), 1 mol% TF-$PI(4,5)P_2$ (blue) and 0.1 mol TF-$PI(4,5)P_2$ loaded with 0.9 mol% non-labeled $PI(4,5)P_2$ (red), in the presence of ~100 μM Ca^{2+}. Inset: fluorescence depolarization profile of similar samples in the absence of Ca^{2+}.

labeled $PI(4,5)P_2$ in POPC GUVs [45]. The sensitivity of TF-$PI(4,5)P_2$ diffusion to calcium suggests once more that cluster size should be significantly higher than just dimers, since in this case, no significant changes in diffusion were expected, as inferred from models of protein diffusion in membranes [50]. Additionally, the determined diffusion coefficients correspond to a mixture of $PI(4,5)P_2$ monomers and clusters within the GUVs, what suggests that clusters may present an even slower diffusion. When compared to POPS, $PI(4,5)P_2$ is also more sensitive to calcium in this range of concentrations. Despite the decrease in the diffusion coefficient recovered for TF-POPS at higher calcium concentrations, at 20 μM Ca^{2+} TF-POPS diffusion remained unaffected.

Altogether, these results indicate that, at physiological $PI(4,5)P_2$ and Ca^{2+} concentrations, Ca^{2+} is capable of promoting $PI(4,5)P_2$ clustering in fluid lipid bilayers. Furthermore, these aggregates are apparently sufficiently large to drastically perturb the lateral distribution of the inositol.

3.3. Effect of Ca^{2+} in the l_o/l_d partition of TF-$PI(4,5)P_2$

The effect of calcium on the apparent liquid ordered (l_o)/liquid disordered (l_d) partition coefficient of $PI(4,5)P_2$ was determined through fluorescence lifetime data of TF-$PI(4,5)P_2$ in the POPC:PSM:Chol mixture (Fig. 6A). The use of the POPC:PSM:Chol lipid mixture for the $PI(4,5)P_2$ partition studies is based on the physiological relevance of phase separation in this system, since membrane rafts are enriched in cholesterol and sphingomyelin and have a low concentration of phospholipids with unsaturated acyl chains [51]. In fact, several reports suggest that $PI(4,5)P_2$ pools exist in the plasma membrane associated with cholesterol-enriched microdomains [24,25], likely allowing the trigger and/or regulation of several $PI(4,5)P_2$-dependent membrane-associated processes through protein–lipid interactions [5,52,53]. Membrane compositions corresponding to different fractions of l_o and l_d phases along a tie line were obtained from a published phase diagram for this composition [54] and partition experiments were carried out at only 0.2 mol% total $PI(4,5)P_2$ to prevent changes in this phase diagram of the ternary mixture.

TF-$PI(4,5)P_2$ fluorescence was only moderately sensitive to the lipid phase in the absence of calcium, suggesting that partition to the l_o phase in the absence of calcium does not induce $PI(4,5)P_2$ clustering. On the other hand, in the presence of physiological concentrations of calcium, a much shorter fluorescence lifetime is obtained for TF-$PI(4,5)P_2$ in the l_o phase, suggesting that calcium induced $PI(4,5)P_2$ clustering is potentiated in liquid ordered domains. Accordingly, a significant change in the fluorescence emission spectrum of TF-$PI(4,5)P_2$ occurs in the l_o phase in the presence of calcium, reflecting the already discussed energy transfer between TF-$PI(4,5)P_2$ molecules (Fig. 6B). Since a fluorescence lifetime difference is observed for TF-$PI(4,5)P_2$ in the l_o and l_d phases, an apparent partition coefficient can be recovered from the variation of $\overline{\tau}$ as the lipid composition changes along a tie line in the phase coexistence region [55] (Fig. 6A).

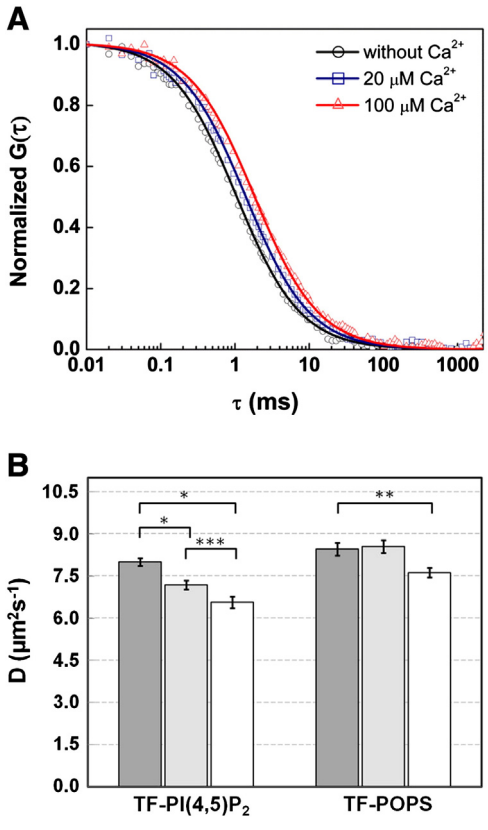

Fig. 5. Ca^{2+}-induced clustering of TF-PI(4,5)P_2 molecules is distinguishable by FCS. Point FCS measurements carried out on the top of immobilized POPC GUVs containing 0.002 mol% TF-PI(4,5)P_2 and unlabeled PI(4,5)P_2 to achieve 1 mol% of total PI(4,5)P_2. (A) Representative normalized autocorrelation curves (full lines are fittings of Eq. (5)), obtained in the absence (○) and presence of 20 μM (□) and 100 μM (△) of Ca^{2+} are depicted. (B) Diffusion coefficients for either TF-PI(4,5)P_2 and TF-POPS were obtained in the absence (dark gray) and presence of 20 μM (light gray) and 100 μM Ca^{2+} (white) ($^*p < 0.001$, $^{**}p < 0.01$, $^{***}p < 0.05$). Values represent means ± standard errors. Diffusion coefficient values for each condition are averages of at least six different GUVs.

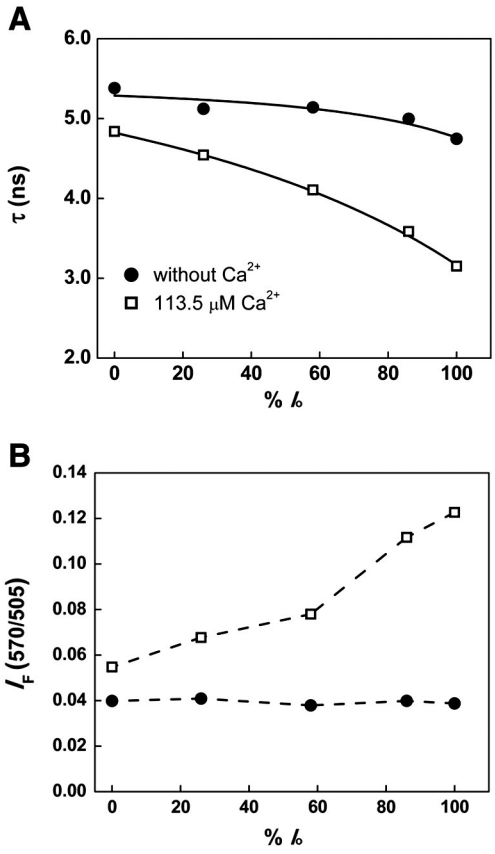

Fig. 6. Ca^{2+} induces a significant increase in PI(4,5)P_2 affinity for l_o membranes. (A) Amplitude-weighted lifetime measured as a function of l_o phase molar fraction in POPC:PSM:Chol membranes containing 0.2 mol% TF-PI(4,5)P_2, in the absence (●) and presence of 113.5 μM Ca^{2+}(□). l_o molar fractions were accomplished following the l_o/l_d tie line of the ternary (POPC:PSM:Chol) phase diagram [54]: 0% l_o (71.6:23.3:5), 26% l_o (59.7:26.3:14), 58% l_o (45.1:29.9:25), 86% l_o (34:32.7:33.3) and 100% l_o (25.4:34.8:39.8). Solid lines are fittings of Eq. (6) to the data, with recovered $K_{p_{app}}^{ld/lo}$ values of 1.9 and 3.6 in the presence and absence of Ca^{2+}, respectively. (B) Spectral change in the fluorescence emission spectrum of TF-PI(4,5)P_2 (reported by I_F(570/505)) as a function of the l_o phase molar fraction, in the absence (●) and presence of 113.5 μM Ca^{2+}(□). Dashed lines are guides to the eye.

Liquid disordered/liquid ordered partition coefficients ($K_p^{(ld/lo)}$) for TF-PI(4,5)P_2 in the presence and absence of calcium were recovered from Eq. (6) [55]:

$$\overline{\tau} = \frac{K_p^{lo/ld}\overline{\tau}_{lo}X_{lo} + \overline{\tau}_{ld}X_{ld}}{K_p^{lo/ld}X_{lo} + X_{ld}} \quad 6$$

where $\overline{\tau}_{lo}$ and $\overline{\tau}_{ld}$ are the amplitude-weighted lifetimes in pure l_o and l_d phases, respectively, and X_i are the molar fractions of l_o and l_d phase in each composition. This partition coefficient is an apparent value, since it refers to the average behavior of both monomeric and clustered molecules. Partition coefficient values of $K_{p_{app}}^{ld/lo} = 1.9$ and 3.6 were recovered in the presence and absence of calcium, respectively. Calcium clearly shifted the average partition properties of PI(4,5)P_2 molecules towards a more moderate preference for the l_d phase. Since these results correspond to a mixture of monomeric and clustered PI(4,5)P_2 species, and the partition properties of the monomeric lipid are not expected to be changed in the presence of calcium, it is reasonable to expect that the observed change reflects the behavior of the clustered molecules. In this case, it is highly likely that clustered PI(4,5)P_2 has an even greater affinity for l_o phases.

The above determined values for the partition coefficient rely on the study of the variation of the amplitude-weighted fluorescence lifetime, along a tie-line of the ternary lipid system (Eq. (6)). This tie-line and the phase boundaries were as described obtained from a published phase diagram for this composition [54]. Although different phase diagrams are also available for this lipid mixture [56–58], the discrepancies between them are mainly found in the low PSM concentration range, and the tie-line used is far away from this region, crossing the center of the triangle (1:1:1 composition), where there is agreement in the literature regarding l_d/l_o co-existence.

4. Discussion

The ability of calcium to induce segregation of PI(4,5)P_2 into clusters has been previously demonstrated mainly through microscopy techniques at non-physiological (at very high concentrations of either the divalent ion and the inositol) or near-physiological conditions [20–23]. For more physiologically relevant concentrations of PI(4,5)P_2 and Ca^{2+} ([PI(4,5)P_2] ≤ 1 mol%; [Ca^{2+}] = 0.1–100 μM), clustering was only observed on supported lipid monolayers [23]. Still, it has not been clarified if cluster formation would occur for free-standing bilayers under more physiologically relevant conditions.

As shown here, PI(4,5)P_2 clusters are not detectable through confocal microscopy of GUVs composed of POPC:PI(4,5)P_2 99:1 (mol:mol) under physiological concentrations of calcium. Wang and coworkers [23] showed that the dimensions of PI(4,5)P_2 clusters formed in the presence of calcium in lipid monolayers were highly dependent on the molar fraction of PI(4,5)P_2 in the membrane, and for very high concentrations of PI(4,5)P_2 (10%), clusters were found to have an average size of 40 nm. In this way, under lower and physiological concentrations of the phosphatidylinositol, clusters are expected to

present dimensions below the resolution of traditional microscopy techniques.

The spectroscopic characterization of fluorescent labeled $PI(4,5)P_2$ molecules have been used before in the study of protein–lipid interactions. These probes have shown that some $PI(4,5)P_2$ binding membrane proteins are able to sequester several $PI(4,5)P_2$ molecules [59] while others are not [60]. Here, we employed similar methodologies to the detection of $PI(4,5)P_2$ clusters in lipid bilayers under physiological concentrations of $PI(4,5)P_2$ and calcium. Ca^{2+} mediated clustering of $PI(4,5)P_2$ in these conditions was confirmed through several different approaches which included information on quantum yield, fluorescence anisotropy, fluorescence spectra and diffusion properties of a fluorescent derivative of $PI(4,5)P_2$, TF-$PI(4,5)P_2$. Experiments with unlabeled $PI(4,5)P_2$ clearly showed that clustering was not a result of phospholipid labeling. Importantly, calcium mediated $PI(4,5)P_2$ clustering is shown to be insensitive to the concentration of a polyamine, suggesting a higher affinity of $PI(4,5)P_2$ for calcium than for polyamines. This specificity of $PI(4,5)P_2$ for interaction with calcium is likely to be important for achieving fast and efficient cellular responses to changes in intracellular calcium levels.

It is clear from the fluorescence depolarization data that clusters must be significantly larger than small oligomers (>2–4 molecules), as the inclusion of unlabeled $PI(4,5)P_2$ promoted clustering between TF-$PI(4,5)P_2$ molecules. Using a model for fluorescence depolarization which assumed a fixed $PI(4,5)P_2$ cluster size for the different calcium concentrations, we concluded that the average cluster size was approximately 15 molecules, although this value is expected to be dependent on both $PI(4,5)P_2$ and calcium concentrations. The presence of significantly large $PI(4,5)P_2$ clusters is supported by FCS data obtained in GUVs composed of POPC:$PI(4,5)P_2$ 99:1 (mol:mol), since a decrease in $PI(4,5)P_2$ diffusion coefficients under calcium concentrations as low as 20 μM was observed and such a decrease is not expected to occur for very small aggregate formation (e.g. dimers). The fact that we are measuring the diffusion of a mixture of monomers and clusters of $PI(4,5)P_2$ molecules suggests an even slower diffusion for the clusters alone. Controls for all experiments were also performed with TF-POPS, in order to guarantee that any effects observed were specific to $PI(4,5)P_2$. The fluorescence of TF-POPS was insensitive to calcium for all experiments performed, under all calcium and POPS concentrations. The only exception was the diffusion coefficient of TF-POPS in GUVs composed of POPC:POPS 99:1 (mol:mol), which appeared to decrease to some extent (although not as much as $PI(4,5)P_2$) at the maximum calcium concentration tested. Still, at a $[Ca^{2+}] = 20$ μM, the diffusion coefficient of TF-POPS remained unchanged. It is possible that calcium at high concentrations does change the diffusion properties of POPS to some extent, and this was previously observed for higher calcium concentrations [61]. Nevertheless, it is clear that calcium at physiological concentrations does not induce clustering of POPS, as this would have been detected from the other experimental approaches.

In this way, the lateral distribution of $PI(4,5)P_2$ presents significant sensitivity to changes in calcium concentration of only a few micromolar. $PI(4,5)P_2$ has been shown to be essential for different cellular functions, including SNARE mediated exocytosis. In this particular case, it is expected that localized increases in calcium concentration will dramatically change the pattern of $PI(4,5)P_2$ lateral distribution and interaction with synaptic proteins, possibly enhancing fusion rates and promoting exocytosis. It is possible that calcium mediated $PI(4,5)P_2$ clustering generates specific sites in the membrane highly enriched with this inositol while depleting the bulk of the membrane, and attracting in this way different protein partners to very specific sites in the plasma membrane. Alternatively, calcium might compete for $PI(4,5)P_2$ binding with $PI(4,5)P_2$-binding membrane proteins, modulating their activity. In fact, a large pool of $PI(4,5)P_2$ in the plasma membrane is thought to be buffered by interactions with membrane proteins [59]. Recently, $PI(4,5)P_2$ was shown to increase synaptotagmin sensitivity for Ca^{2+} in vitro more than 40-fold [8], suggesting that $PI(4,5)P_2$ can also work as an anchor for calcium ions in the membrane. In this case, formation of $PI(4,5)P_2$-Ca^{2+} clusters would generate sites in the membrane with dramatically increased calcium concentrations, contributing to the potentiation of local increases in the concentration of the divalent cation.

Additionally, we also showed here that calcium mediated $PI(4,5)P_2$ clustering is significantly more efficient in liquid ordered membranes, and that the $PI(4,5)P_2$-Ca^{2+} clusters present an increased affinity for l_o domains. In this case, lipid rafts could function in the plasma membrane of living cells as nucleators of $PI(4,5)P_2$ clusters after calcium stimulation, providing a higher localization specificity to the process.

5. Conclusions

In this work, we show that under physiological concentrations of calcium and $PI(4,5)P_2$, and in the absence of membrane perturbations, changes in calcium concentration induce dramatic effects on the distribution of $PI(4,5)P_2$ on free-standing lipid bilayers. The dimension of the clusters formed under physiological conditions is expected to vary greatly depending on both calcium and $PI(4,5)P_2$ concentrations, but for 1 mol% $PI(4,5)P_2$ in POPC liposomes, our results could be rationalized on the basis of an average cluster size of 15 $PI(4,5)P_2$ molecules. Calcium mediated $PI(4,5)P_2$ clustering is also shown to be significantly more sensitive in liquid ordered membranes, and $PI(4,5)P_2$-Ca^{2+} clusters present an increased affinity for l_o domains. In this way, the lateral distribution of $PI(4,5)P_2$ presents significant sensitivity to changes in calcium concentration in the physiological range, which is likely to allow this lipid to function as an effective lipidic calcium sensor. The increased efficiency of calcium-mediated $PI(4,5)P_2$ clustering on liquid ordered domains might provide targeted nucleation sites for $PI(4,5)P_2$ clusters upon calcium stimulus.

Acknowledgements

MJS and FF are recipients of fellowships from FCT (SFRH/BD/80575/2011 and SFRH/BPD/64320/2009, respectively). Authors acknowledge funding by FCT project references PTDC/QUI-BIQ/112067/2009, PTDC/QUI-BIO/119494/2010, and PEst-OE/CTM/LA0024/2011.

Appendix A. Supplementary data

Supplementary data to this article can be found online at http://dx.doi.org/10.1016/j.bbamem.2013.11.020.

References

[1] D.E. Clapham, Calcium signaling, Cell 80 (1995) 259–268.
[2] P.L. Greer, M.E. Greenberg, From synapse to nucleus: calcium-dependent gene transcription in the control of synapse development and function, Neuron 59 (2008) 846–860.
[3] E. Neher, Vesicle pools and Ca2+ microdomains: new tools for understanding their roles in neurotransmitter release, Neuron 20 (1998) 389–399.
[4] E. Neher, T. Sakaba, Multiple roles of calcium ions in the regulation of neurotransmitter release, Neuron 59 (2008) 861–872.
[5] K. Aoyagi, T. Sugaya, M. Umeda, S. Yamamoto, S. Terakawa, M. Takahashi, The activation of exocytotic sites by the formation of phosphatidylinositol 4,5-bisphosphate microdomains at syntaxin clusters, J. Biol. Chem. 280 (2005) 17346–17352.
[6] A.D. Lam, P. Tryoen-Toth, B. Tsai, N. Vitale, E.L. Stuenkel, SNARE-catalyzed fusion events are regulated by Syntaxin1A-lipid interactions, Mol. Biol. Cell 19 (2008) 485–497.
[7] D.J. James, C. Khodthong, J.A. Kowalchyk, T.F.J. Martin, Phosphatidylinositol 4,5-bisphosphate regulates SNARE-dependent membrane fusion, J. Cell Biol. 182 (2008) 355–366.
[8] G. van den Bogaart, K. Meyenberg, U. Diederichsen, R. Jahn, Phosphatidylinositol 4,5-bisphosphate increases Ca2+ affinity of synaptotagmin-1 by 40-fold, J. Biol. Chem. 287 (2012) 16447–16453.
[9] K. Kwiatkowska, One lipid, multiple functions: how various pools of PI(4,5)P(2) are created in the plasma membrane, Cell. Mol. Life Sci. 67 (2010) 3927–3946.
[10] J.E. Ferrell, W.H. Huestis, Phosphoinositide metabolism and the morphology of human erythrocytes, J. Cell Biol. 98 (1984) 1992–1998.
[11] D. Raucher, T. Stauffer, W. Chen, K. Shen, S. Guo, J.D. York, et al., Phosphatidylinositol 4,5-bisphosphate functions as a second messenger that regulates cytoskeleton–plasma membrane adhesion, Cell 100 (2000) 221–228.
[12] A. Sechi, J. Wehland, The actin cytoskeleton and plasma membrane connection: PtdIns(4,5)P2 influences cytoskeletal protein activity at the plasma membrane, J. Cell Sci. 113 (2000) 3685–3695.

[13] M.R. Logan, C.A. Mandato, Regulation of the actin cytoskeleton by PIP2 in cytokinesis, Biol. Cell. 98 (2006) 377–388.
[14] A. Honda, M. Nogami, T. Yokozeki, M. Yamazaki, H. Nakamura, H. Watanabe, et al., Phosphatidylinositol 4-phosphate 5-kinase α is a downstream effector of the small G protein ARF6 in membrane ruffle formation, Cell 99 (1999) 521–532.
[15] T.F. Martin, PI(4,5)P(2) regulation of surface membrane traffic, Curr. Opin. Cell Biol. 13 (2001) 493–499.
[16] M.G. Ford, B.M. Pearse, M.K. Higgins, Y. Vallis, D.J. Owen, A. Gibson, et al., Simultaneous binding of PtdIns(4,5)P2 and clathrin by AP180 in the nucleation of clathrin lattices on membranes, Science 291 (2001) 1051–1055.
[17] M. Jost, F. Simpson, J.M. Kavran, M.A. Lemmon, S.L. Schmid, Phosphatidylinositol-4,5-bisphosphate is required for endocytic coated vesicle formation, Curr. Biol. 8 (1998) 1399–1404.
[18] O. Cremona, G. Di Paolo, M.R. Wenk, A. Lüthi, W.T. Kim, K. Takei, et al., Essential role of phosphoinositide metabolism in synaptic vesicle recycling, Cell 99 (1999) 179–188.
[19] I. Milosevic, J.B. Sørensen, T. Lang, M. Krauss, G. Nagy, V. Haucke, et al., Plasmalemmal phosphatidylinositol-4,5-bisphosphate level regulates the releasable vesicle pool size in chromaffin cells, J. Neurosci. 25 (2005) 2557–2565.
[20] K. Carvalho, L. Ramos, C. Roy, C. Picart, Giant unilamellar vesicles containing phosphatidylinositol(4,5)bisphosphate: characterization and functionality, Biophys. J. 95 (2008) 4348–4360.
[21] I. Levental, D.A. Christian, Y.-H. Wang, J.J. Madara, D.E. Discher, P.A. Janmey, Calcium-dependent lateral organization in phosphatidylinositol 4,5-bisphosphate (PIP2)- and cholesterol-containing monolayers, Biochemistry 48 (2009) 8241–8248.
[22] W.G. Ellenbroek, Y.-H. Wang, D.A. Christian, D.E. Discher, P.A. Janmey, A.J. Liu, Divalent cation-dependent formation of electrostatic PIP2 clusters in lipid monolayers, Biophys. J. 101 (2011) 2178–2184.
[23] Y.-H. Wang, A. Collins, L. Guo, K.B. Smith-Dupont, F. Gai, T. Svitkina, et al., Divalent cation-induced cluster formation by polyphosphoinositides in model membranes, J. Am. Chem. Soc. 134 (2012) 3387–3395.
[24] L.J. Pike, J.M. Miller, Cholesterol depletion delocalizes phosphatidylinositol bisphosphate and inhibits hormone-stimulated phosphatidylinositol turnover, J. Biol. Chem. 273 (1998) 22298–22304.
[25] C.M. Johnson, G.R. Chichili, W. Rodgers, Compartmentalization of phosphatidylinositol 4,5-bisphosphate signaling evidenced using targeted phosphatases, J. Biol. Chem. 283 (2008) 29920–29928.
[26] J. Tong, L. Nguyen, A. Vidal, S.A. Simon, J.H.P. Skene, T.J. McIntosh, Role of GAP-43 in sequestering phosphatidylinositol 4,5-bisphosphate to raft bilayers, Biophys. J. 94 (2008) 125–133.
[27] L.D. Mayer, M.J. Hope, P.R. Cullis, Vesicles of variable sizes produced by a rapid extrusion procedure, Biochim. Biophys. Acta 858 (1986) 161–168.
[28] M.I. Angelova, D.S. Dimitrov, Liposome electroformation, Faraday Discuss. Chem. Soc. 81 (1986) 303–311.
[29] R.F.M. de Almeida, J. Borst, A. Fedorov, M. Prieto, A.J.W.G. Visser, Complexity of lipid domains and rafts in giant unilamellar vesicles revealed by combining imaging and microscopic and macroscopic time-resolved fluorescence, Biophys. J. 93 (2007) 539-553.
[30] M.J. Sarmento, M. Prieto, F. Fernandes, Reorganization of lipid domain distribution in giant unilamellar vesicles upon immobilization with different membrane tethers, Biochim. Biophys. Acta 1818 (2012) 2605-2615.
[31] C.W. McClare, An accurate and convenient organic phosphorus assay, Anal. Biochem. 39 (1971) 527–530.
[32] R. Haugland, Handbook of Fluorescence Probes and Research Chemicals, Molecular Probes, Eugene, OR, 1996.
[33] M.M. Puchalski, M.J. Morra, R. von Wandruszka, Assessment of inner filter effect corrections in fluorimetry, Fresen, J. Anal. Chem. 340 (1991) 341–344.
[34] J. Lakowicz, Principles of Fluorescence Spectroscopy, Kluwer Academics, New York, 1999.
[35] L.M. Loura, A. Fedorov, M. Prieto, Partition of membrane probes in a gel/fluid two-component lipid system: a fluorescence resonance energy transfer study, Biochim. Biophys. Acta 1467 (2000) 101–112.
[36] C. Boucheny, G.P. Bonneau, J. Droulez, G. Thibault, S. Ploix, A perceptive evaluation of volume rendering techniques, ACM Trans. Appl. Percept. 5 (2009) 1–24.
[37] P.-O. Gendron, F. Avaltroni, K.J. Wilkinson, Diffusion coefficients of several rhodamine derivatives as determined by pulsed field gradient-nuclear magnetic resonance and fluorescence correlation spectroscopy, J. Fluoresc. 18 (2008) 1093–1101.
[38] N. Kahya, D. Scherfeld, K. Bacia, B. Poolman, P. Schwille, Probing lipid mobility of raft-exhibiting model membranes by fluorescence correlation spectroscopy, J. Biol. Chem. 278 (2003) 28109–28115.
[39] F. Heinemann, V. Betaneli, F.A. Thomas, P. Schwille, Quantifying lipid diffusion by fluorescence correlation spectroscopy: a critical treatise, Langmuir 28 (2012) 13395–13404.
[40] J. Ries, P. Schwille, New concepts for fluorescence correlation spectroscopy on membranes, Phys. Chem. Chem. Phys. 10 (2008) 3487–3497.
[41] M. Dahim, N.K. Mizuno, X.-M. Li, W.E. Momsen, M.M. Momsen, H.L. Brockman, Physical and photophysical characterization of a BODIPY phosphatidylcholine as a membrane probe, Biophys. J. 83 (2002) 1511–1524.
[42] I. Mikhalyov, N. Gretskaya, F. Bergström, L.B.-Å. Johansson, Electronic ground and excited state properties of dipyrromethene boron difluoride (BODIPY): dimers with application to biosciences, Phys. Chem. Chem. Phys. 4 (2002) 5663–5670.
[43] F. Bergström, I. Mikhalyov, P. Hägglöf, R. Wortmann, T. Ny, L.B.Å. Johansson, Dimers of dipyrromethene boron difluoride (BODIPY) with light spectroscopic applications in chemistry and biology, J. Am. Chem. Soc. 124 (2002) 196–204.
[44] F. Fernandes, L.M.S. Loura, A. Fedorov, M. Prieto, Absence of clustering of phosphatidylinositol-(4,5)-bisphosphate in fluid phosphatidylcholine, J. Lipid Res. 47 (2006) 1521–1525.
[45] P.D.J. Moens, E. Gratton, I.L. Salvemini, Fluorescence correlation spectroscopy, raster image correlation spectroscopy, and number and brightness on a commercial confocal laser scanning microscope with analog detectors (Nikon C1), Microsc. Res. Tech. 388 (2010) 377–388.
[46] F. Fernandes, L.M.S. Loura, M. Prieto, R. Koehorst, R.B. Spruijt, M.A. Hemminga, Dependence of M13 major coat protein oligomerization and lateral segregation on bilayer composition, Biophys. J. 85 (2003) 2430–2441.
[47] M.N. Berberan-Santos, M.J.E. Prieto, Energy transfer in spherical geometry, J. Chem. Soc. Faraday Trans. 2. 83 (1987) 1391–1409.
[48] B. Snyder, E. Freire, Fluorescence energy transfer in two dimensions. A numeric solution for random and nonrandom distributions, Biophys. J. 40 (1982) 137–148.
[49] L.W. Runnels, S.F. Scarlata, Theory and application of fluorescence homotransfer to melittin oligomerization, Biophys. J. 69 (1995) 1569–1583.
[50] G. Saffman, M. Delbrock, Brownian motion in biological membranes, Proc. Natl. Acad. Sci. U. S. A. 72 (1975) 3111–3113.
[51] J. Silvius, Role of cholesterol in lipid raft formation: lessons from lipid model systems, Biochim. Biophys. Acta 1610 (2003) 174–183.
[52] T. Laux, K. Fukami, M. Thelen, T. Golub, D. Frey, P. Caroni, GAP43, MARCKS, and CAP23 modulate PI(4,5)P(2) at plasmalemmal rafts, and regulate cell cortex actin dynamics through a common mechanism, J. Cell Biol. 149 (2000) 1455–1472.
[53] G. van den Bogaart, K. Meyenberg, H.J. Risselada, H. Amin, K.I. Willig, B.E. Hubrich, et al., Membrane protein sequestering by ionic protein–lipid interactions, Nature 473 (2011) 4–7.
[54] R.F.M. de Almeida, A. Fedorov, M. Prieto, Sphingomyelin/phosphatidylcholine/cholesterol phase diagram: boundaries and composition of lipid rafts, Biophys. J. 85 (2003) 2406–2416.
[55] L.C. Silva, R.F.M. de Almeida, B.M. Castro, A. Fedorov, M. Prieto, Ceramide-domain formation and collapse in lipid rafts: membrane reorganization by an apoptotic lipid, Biophys. J. 92 (2007) 502–516.
[56] R.S. Petruzielo, F. a Heberle, P. Drazba, J. Katsaras, G.W. Feigenson, Phase behavior and domain size in sphingomyelin-containing lipid bilayers, Biochim. Biophys. Acta 1828 (2013) 1302–1313.
[57] I.V. Ionova, V. a Livshits, D. Marsh, Phase diagram of ternary cholesterol/palmitoylsphingomyelin/palmitoyloleoyl-phosphatidylcholine mixtures: spin-label EPR study of lipid-raft formation, Biophys. J. 102 (2012) 1856–1865.
[58] A. Pokorny, L.E. Yandek, A.I. Elegbede, A. Hinderliter, P.F.F. Almeida, Temperature and composition dependence of the interaction of delta-lysin with ternary mixtures of sphingomyelin/cholesterol/POPC, Biophys. J. 91 (2006) 2184–2197.
[59] A. Gambhir, G. Hangyás-Mihályné, I. Zaitseva, D.S. Cafiso, J. Wang, D. Murray, et al., Electrostatic sequestration of PIP2 on phospholipid membranes by basic/aromatic regions of proteins, Biophys. J. 86 (2004) 2188–2207.
[60] G. Blin, E. Margeat, K. Carvalho, C. a Royer, C. Roy, C. Picart, Quantitative analysis of the binding of ezrin to large unilamellar vesicles containing phosphatidylinositol 4,5 bisphosphate, Biophys. J. 94 (2008) 1021–1033.
[61] R. Gilmanshin, C.E. Creutz, L.K. Tamm, Annexin IV reduces the rate of lateral lipid diffusion and changes the fluid phase structure of the lipid bilayer when It binds to negatively charged membranes in the presence of calcium, Biochemistry 33 (1994) 8225–8232.